Free Volume and Density Gradients of Amorphous Polymer Surfaces As Determined by Use of a Pulsed Low-Energy Positron Lifetime Beam and PVT Data

John Algers,[†] Ryoichi Suzuki,[‡] Toshiyuki Ohdaira,[‡] and Frans H. J. Maurer*,[†]

Polymer Science & Engineering, Lund Institute of Technology, Lund University, SE-221 00 Lund, Sweden, and Electrotechnical Laboratory, Tsukuba-shi, Ibaraki 305-8568, Japan

Received December 17, 2003; Revised Manuscript Received March 12, 2004

ABSTRACT: Density gradient widths at the polymer−vacuum surfaces of poly(methyl methacrylate), styrene-*co*-acrylonitrile, and styrene-*co*-maleic anhydride were quantified to 2, 5, and 4 nm, respectively, by use of a pulsed low-energy positron lifetime beam and to approximately 1.5 nm for all three polymers on the basis of theoretical predictions from pressure−volume−temperature (PVT) data, making use of the Cahn−Hilliard theory of inhomogeneous systems in conjunction with the Sanchez−Lacombe lattice fluid theory. Excellent agreement between the two methods was found for the homopolymer, whereas for the copolymers, the former method gave larger density gradient widths, a result attributed to the surface orientation of the less polar polymer segments, which the theoretical predictions did not take into account. As has been previously proposed, the discrepancy between the depth ranges of the surface effects on density and the glass transition temperature (T_g) is suggested to result from a coupling between the dynamics of adjoining polymer segments, canceling a direct relationship between local density profile $\rho(z)$ and local $T_g(z)$ as a function of distance z from the free surface.

Introduction

The properties of polymer surfaces have attracted increasing attention in polymer physics, both as topics of fundamental research aimed at understanding the thermodynamics of surfaces and in applied research concerned with such issues as adhesion, compatibility, and wettability of polymers. Most experimental work has been performed on thin supported polymer films, often aimed at resolving the thermal properties in the near-surface region close to the vacuum or air interface. Some of the first systematic experiments involved measurements of the thermal expansivity of thin polymer films, spin-cast on top of a substrate, using X-ray reflectivity[1] or ellipsometry.[2,3] Since then, a variety of instruments have been used in similar experiments, most commonly ellipsometry[4−9] and X-ray reflectivity[6,10,11] but also Brillouin light scattering,[12,13] neutron reflectrometry,[14,15] optical waveguide spectroscopy,[16] and dielectric loss measurements.[17−19] Typically, the thermal expansivities and glass transitions are studied as a function of film thickness and, in some cases, as a function of molecular mass and substrate. Most experimental results agree on there being a reduction in the glass transition temperature (T_g) with decreasing thickness of the thin supported films, unless a strong polymer−substrate interaction occurs.

An important issue has been the influence of the polymer−substrate interaction on the overall thin-film properties. Since the above-mentioned techniques are normally sensitive to the total film thickness only, and thus to the total thermal expansivity of the sample, they measure some average of the properties of the near-surface region, the near-substrate region, and for thicker films an intermediary bulklike region. Studies of the near-surface region using thin supported films may thus be hampered by the influence of the substrate−polymer interaction. In 1996, Forrest et al. measured the T_g in free-standing polystyrene films,[12] in this way eliminating any substrate effects. The T_g of the free-standing films was found then to produce a larger reduction in the T_g than had been observed previously for supported films of comparable thickness.[12,13,20] This observation led to the conclusion that some of the earlier investigations of the T_g of thin supported polymer films were strongly influenced by substrate effects. More recently, in a systematic study of the influence of the polymer−substrate interaction, it was found that the T_g could either increase or decrease in comparison to its bulk value, depending on the interfacial energy between the polymer and substrate. Accordingly, it was suggested that the shift of the T_g from its bulk value was indeed directly correlated to the interfacial energy between the substrate and the polymer.[6]

To separate the contributions of the free surface and the polymer−substrate interface to the average properties of thin supported films, layer models have been proposed.[2,3,18,20,21] Such models have been used to explain the change in T_g in very thin films in terms of the presence of a near-surface layer of increased mobility. Estimates of the width of the near-surface layer ranges from 2 to 15 nm, its thickness being dependent upon the details of the model used, as well as the temperature, molecular mass, molecular structure, and the experimental technique. For polystyrene, the width of the mobile layer was suggested to be temperature dependent and its average thickness to be approximately 8 nm in the glassy state,[3] and for PMMA it was found from similar measurements made by the same group to be even larger.[2] Dielectric loss experiments of polystyrene, in close agreement with these measurements, have indicated there to be a 7.5 nm near-surface layer.[18] More recently, Forrest et al. suggested there is a mobile layer of temperature-dependent thickness,

[†] Lund Institute of Technology.
[‡] Electrotechnical Laboratory.
* Corresponding author: Tel +46 462229149, Fax +46 462224115; e-mail frans.maurer@polymer.lth.se.

10.1021/ma0359335 CCC: $27.50
Published on Web 04/30/2004

which for polystyrene at room temperature is approximately 11 nm thick,[20] in good agreement the 10 nm thick layer later suggested by Kawana et al.[9]

Contact-mechanical experiments represent quite a different strategy for studying free polymer surfaces, one which avoids many of the problems connected with thin supported films. Scanning force microscopy, in which the viscoelastic properties of the near-surface region can be probed as a function of temperature,[22−28] molecular mass,[22,24,26,28−30] film thickness, and frequency,[25] is the most commonly used method. In some investigations[22,23,26−29] a reduction of T_g, or an increase in mobility, has been found in the near-surface region while other studies have suggested there to be a bulklike T_g at the surface.[24,25] Since this disagreement between research groups has been attributed to differences in experimental conditions, such as the shape, size, and stiffness of the tip used for the scanning probe experiments,[24,31] the thrust of the experimental results is not conclusive at present. The glass transition, the increase in mobility, and other aspects of thin polymer films, as well as the multitude of experimental techniques that have been used to measure them, have been reviewed extensively.[31−34]

The reduction in T_g usually found in thin polymer films suggests there to be a surface layer of increased mobility, implying that the free volume is larger in the near-surface region than in the bulk state of the polymer. The problem of discerning whether the shift in the T_g in thin polymer films arises from an increase in free volume in the near-surface region appears ideally suited for low-energy positron beam studies,[35,36] which can yield depth-resolved information on the free volume characteristics in polymers.

In pulsed low-energy positron annihilation spectroscopy, positrons are implanted as a function of implantation energy E in the range of approximately 0.3−20 keV, with a median implantation depth range in polymers of approximately 4−3000 nm. The free volume characteristics of the polymer are obtained from the positron annihilation lifetime spectra as a function of depth. Recently, we studied in some detail the positron implantation characteristics in amorphous polymers, the result being found to be in excellent agreement with previously published data on metals, using mass density as the only scaling parameter.[37]

In 1995, Xie et al. reported one of the first systematic investigations of the free volume characteristics of a free polymer surface.[38] This involved measuring the positron annihilation lifetime in the implantation energy range of 0.3−6 keV in thin supported films. A variety of different polymers were measured. The authors were unable to resolve an increase in the free volume size close to the surface. Further studies by the same group,[21] however, revealed appreciable surface and substrate effects on the thermal expansivities of polystyrene spin-coated onto silicon substrates. A three-layer model was proposed, including a near-surface layer of reduced T_g and a thickness of about 2 nm. A reduction in T_g at the free surface was also found by Jean et al. by use of the Doppler broadening of the energy spectra in positron annihilation,[39] the T_g of polystyrene being found to be 57 °C below the bulk level at a location 5 nm from the vacuum surface. Similar results of low-energy positron lifetime experiments have been obtained in more recent positron lifetime studies of polystyrene[40] and epoxy polymer.[41] A number of isothermal investigations of a variety of polymer materials,[42] including epoxy polymer,[43] polyurethane,[44] polystyrene,[45] polypropylene,[46] and low-density polyethylene,[47,48] have shown there to be a rather large increase in free volume size close to the free surface at room temperature, in contrast to what was previously found for polystyrene.[38] However, differences in the evaluation methods applied to the data may account for some of the discrepancy between the free volume estimates, especially in the case of polystyrene.[38,45]

The depth range of the free volume size increase as measured by positron lifetime experiments is in basic agreement with the idea of a near-surface mobile layer of reduced T_g. It is instructive, however, to compare positron lifetime results with density measurements of thin polymer films, since in amorphous polymers, there is a strong correlation between free volume and density. Surprisingly enough, other experiments aimed at measuring the density of thin polymer films suggest the density to be independent of film thickness and to be consistent with bulk density, even for very thin films. Twin neutron reflectivity[49] has shown the density of thin films of polystyrene spin-coated onto silicon substrates to be the same as that for bulk polystyrene, independent of the film thickness. The thinnest film was 6.5 nm thick, which is of the same order of magnitude as the thickness of the near-surface mobile layer proposed previously by several groups. Brillouin light scattering[50] has been used as an indirect but sensitive probe of mass density in free-standing polymer films. In agreement with previous neutron reflectivity measurements of supported films, no significant change in density was observed for the free-standing films, the thinnest film being 29 nm thick. The drastic reductions in T_g in free-standing films previously observed by the same group, e.g., −60 K for a 29 nm film,[12,13] could thus not be explained by a reduction in density of a near-surface layer, an observation which immediately raises some interesting questions concerning the relations in polymer surfaces between free volume and mobility.

In conclusion, one can state that the effects on density in thin polymer films appears to be very small and that the commonly observed reduction in T_g in thin polymer films does not appear to be resulting from a reduction of the density at the same depth from the surface. In this context, free volume characterization of polymer surfaces by use of positrons would provide useful additional information. However, to the best of the authors' knowledge, the results of free volume characterization by use of low-energy positron techniques have thus far been reported in quantities which are not directly comparable to density gradients.

The aim of the present study was to use a pulsed low-energy positron beam to measure the free volume characteristics at the near-surface region of amorphous polymers and to investigate whether the results can be interpreted in terms of a simple density gradient. Three amorphous polymers with previously well-characterized free volume properties in the bulk state were selected:[51,52] poly(methyl methacrylate) (PMMA), poly(styrene-*co*-acrylonitrile) (SAN), and poly(styrene-*co*-maleic anhydride) (SMA). Use of thick films (of about 1 μm) should result in small effects of the substrate−polymer interaction on the near-surface region.

Previously determined pressure−volume−temperature (PVT) data on all three polymers allowed theoretical density gradients to be calculated from the Cahn−

Hilliard theory of inhomogeneous systems[53] in conjunction with the lattice fluid model of Sanchez−Lacombe[54,55] and to then be compared with the results of the positron beam experiments.

Experimental Section

Three amorphous polymers with similar glass transition temperatures were chosen for the study: atactic poly(methyl methacrylate) (PMMA), (Scientific Polymer Products cat#037B, M_w = 75 kg/mol), poly(styrene-*co*-acrylonitrile) (SAN) (25 wt % AN, BASF AG type 358N, M_w = 170 kg/mol), and poly(styrene-*co*-maleic anhydride) (SMA) (14 wt % MA, Monomer-Polymer & Dajacs Lab cat# 8097, M_w = 50 kg/mol). Silicon wafers, doped with phosphorus to a concentration of approximately 10^{14} cm^{-3} (Topsil, CFZ N (100) 4 in.), were cut into 15 × 15 mm pieces and used as substrates for the polymer films.

The polymer films were prepared by spin-coating.[56] To obtain polymer solutions suitable for spin-coating, PMMA was dissolved in toluene and SAN and SMA in 1,2-dichloroethane to concentrations of between 66 and 100 mg/mL. The polymer film samples were spin-coated onto the silicon substrates at 2000 rpm in ambient atmosphere. After spin-coating, the films were dried at 160 °C in a vacuum for 12 h to ensure both evaporation of the solvent and a well-defined equilibrium state of the films, which were then cooled at 0.5 °C/min to room temperature. The thickness and quality of the films were measured by atomic force microscopy (AFM) in contact mode. The thickness of the films was found to be in the range 1−1.2 μm and the surface to be very smooth, free of any appreciable defects caused by solvent evaporation.

Positron lifetime spectra were recorded in the energy range 0.3−5 keV, using a pulsed, low-energy positron system[36] with a BaF_2 detector. The energy-dependent time resolution of the apparatus was approximately 490 ps at 0.3 keV, decreasing as a function of energy to a constant level of about 280 ps at 1.0 keV and at higher energies. About 1 million counts or more were collected for each spectrum. The peak-to-background ratio was 1 × 10^3 at 0.3 keV, increasing to 5 × 10^3 at 2 keV and above. The spectra were evaluated by PATFIT[57] with use of a one-Gaussian resolution function. Three lifetimes were used in the evaluation, τ_1, τ_2, and τ_3 with the corresponding relative intensities I_1, I_2, and I_3. Each lifetime in the evaluation corresponds to a different type of positron annihilation. The shortest lifetime, τ_1, is the lifetime of parapositronium (p-Ps), consisting of a positron and an electron with antiparallel spins, τ_2 is the lifetime of free positrons, and τ_3 is the lifetime of orthopositronium (o-Ps), consisting of a positron and electron with parallel spins. In polymers, the o-Ps lifetime τ_3 is dependent on the free volume size according to the Tao−Eldrup equation[58,59]

$$\tau_3 = \frac{1}{2}\left[1 - \frac{R}{R_0} + \frac{1}{2\pi}\sin\left(\frac{2\pi R}{R_0}\right)\right]^{-1} \quad (1a)$$

$$V(\tau_3) = \frac{4\pi R^3}{3} \quad (1b)$$

where τ_3 is expressed in ns and R is the radius of a hypothetical spherical free volume cavity in Å, surrounded by an electron layer of thickness $R_0 - R$ = 1.656 Å.

Results

Spectra of PMMA are plotted in Figure 1. For sake of clarity, only three positron implantation energies are displayed: two near-surface spectra of 0.3 and 0.7 keV and one spectrum of 3.0 keV representing a "bulk" spectrum in which the free surface has negligible influence.

The main difference between the spectra in the 10−30 ns region results primarily from the increase in background level with decreasing implantation energy.

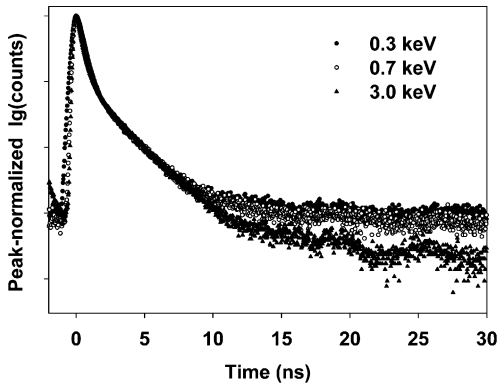

Figure 1. Positron lifetime spectra of PMMA measured with a pulsed low-energy positron beam. The spectra are recorded at implantation energies of 0.3 (●), 0.7 (○), and 3 keV (▲) , having nominal median implantation depths of 3, 13, and 155 nm, respectively.[37]

The spectra of SAN and SMA, which are very similar to those of PMMA, are not shown in figure. All the spectra at E > 0.5 keV displayed a background signal that was energy-dependent but was the same for all the polymers. This could be established by plotting the spectra of the three different polymers, together with reference spectra of Kapton. A background subtraction method was investigated in which the background signal of the Kapton spectra was subtracted from the sample spectra measured at the same energy. However, the changes in the fitting parameters of the subtracted spectra were found to be too small to justify such a procedure. Also, a long-lifetime component of 10% intensity was present in the Kapton spectra at 0.3 and 0.4 keV, thus preventing an evaluation of the true background at these implantation energies. Consequently, no background subtraction was employed in the final evaluation.

Figure 2a−f displays the lifetimes and intensities obtained from a three-lifetime analysis, τ_1 being fixed to 0.125 ns.

As can be seen in Figure 2a, PMMA displays only a weak effect of τ_3 in the near-surface region. Only at the lowest implantation energy 0.3 keV, with a nominal median implantation depth[37] of 3 nm, can a clear increase in the o-Ps lifetime of about 100 ps be distinguished from the bulklike spectra found at higher implantation energy. The effect on τ_3 is somewhat more distinct in SAN and SMA than in PMMA, the increase being approximately 400 and 300 ps, respectively. Previous measurements on an epoxy polymer yielded a similar increase in τ_3 close to the surface,[43] although a considerably larger increase in the order of several nanoseconds has been found for polystyrene[45] and polyurethane.[44]

The o-Ps lifetimes in the energy range of E > 1 kV shown in Figure 2 agree well with the lifetimes and intensities obtained from measurements on the same materials by use of conventional fast−fast coincidence PALS.[51,52] Also, in this energy range the ratio of I_1 to I_3 is approximately 1:3, in close agreement with the relative theoretical formation probabilities of the two types of positronium.

In the range of E < 1 keV, the intensities of all three materials are strongly energy-dependent. The main effects are that at low implantation energy I_1 and I_3 decrease with a corresponding increase in I_2. The reduction in I_1 and I_3 suggests a decrease in the

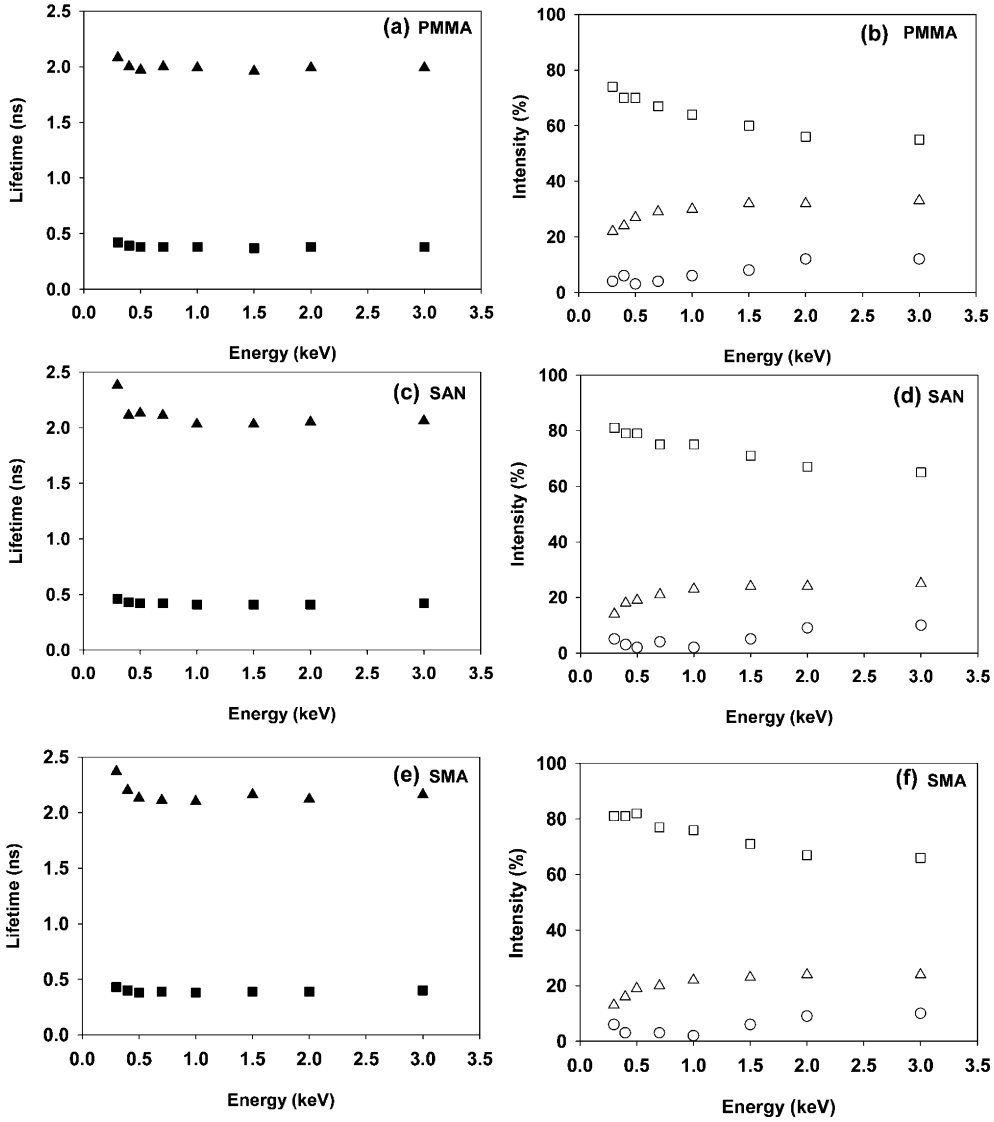

Figure 2. Positron lifetimes and intensities of PMMA, SAN, and SMA in the implantation energy range of 0.3−3 keV. Shown in the graphs to the left are the lifetimes τ_2 (■) and τ_3 (▲). τ_1 was fixed to 0.125 ns in the evaluation and is not displayed. The intensities I_1 (○), I_2 (□), and I_3 (△) are plotted in the graphs to the right.

probability of positronium formation at low implantation energies. The same observation has been made in a number of previous publications,[38,40,43−45] although conflicting interpretations of the decrease have been suggested.

I_3 decreases continuously at low energies and approaches zero at $E = 0$ keV. In contrast to the smooth behavior of I_3 throughout the full energy range, I_1 and I_2 are less regular in the low-energy range, and the ratio of I_1 to I_3 becomes less than 1:3 since I_1 approaches zero prior to I_3. In view of the time resolution of the spectra found in this energy range being up to 4 times as large as the fixed value of 0.125 ns for τ_1, the values of I_1 in this region cannot be expected to provide more than a rough indication of the p-Ps intensity.

Theoretical Calculations. The positron beam data were used, together with previously determined positron implantation characteristics treated as a function of energy and density, to characterize a corresponding density gradient at the free surface in units of mass density ρ vs distance z, $\rho(z)$. This allowed the results of the positron beam measurements to be compared with those of other techniques and predictions.

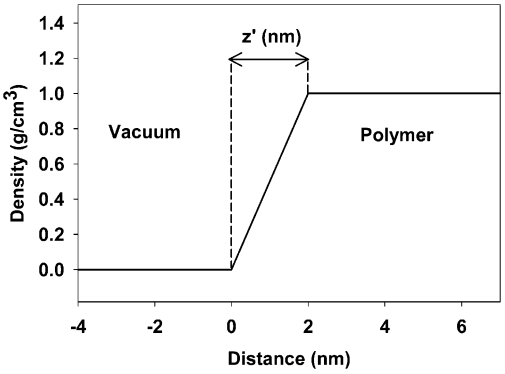

Figure 3. A linear density gradient model was fitted to the positron lifetime data. z' in nm is the width of the gradient and was the only free parameter in the fitting procedure.

A density gradient of the simplest possible shape, i.e., with a linearly increasing density from zero to the polymer bulk value, was fitted to the data (Figure 3).

The linear density gradient can be completely defined by its characteristic width, z', which then is the only free parameter in the fitting.The shape of a model density gradient has an effect on the calculated width,

and there are clearly several shapes other than linear that would yield either a smaller or a larger width. To date, there is very little published experimental data to indicate details of the shape of density gradients at polymer surfaces. Thus, use of a linear density gradient is mainly justified by simplicity, allowing it to be completely defined by one single free-fitting parameter, and on its close similarity to the sigmoidal shape of the density gradients found both by Monte Carlo simulations and by the use of the theoretically predicted density gradient obtained from PVT data, as will be shown below.

The relationship between the density gradient and the experimental lifetime as a function of the implantation energy was assumed to be described by eq 2, which states that the experimentally determined o-Ps lifetime obtained from each spectrum is an average of the local o-Ps lifetimes in the positron implantation probe. The local o-Ps lifetime is a function of the density gradient $\rho(z)$ (eq 6). Equations 3−7 describe the positron implantation characteristics of amorphous polymers, as has been investigated previously.[37] Equation 7 describes the median implantation depth $z_{1/2}$ in units of nm for implantation energies in units of kiloelectronvolts.

$$\tau_3(E) = \int_{z=-\infty}^{z=\infty} P(z,E)\, \tau_3(z)\, \mathrm{d}z \tag{2}$$

$$\tau_3(z) = f\{\rho(z)\} \tag{3}$$

$$P(z,E) = -\frac{\mathrm{d}}{\mathrm{d}z}\left\{\exp\left[-\left(\frac{z}{z_0\{E,\rho(z)\}}\right)^m\right]\right\} \tag{4}$$

$$P(z,E) = \frac{m z^{m-1}}{{z_0}^m\{E,\rho(z)\}} \exp\left[-\left(\frac{z}{z_0\{E,\rho(z)\}}\right)^m\right] \tag{5}$$

$$z_0(E) = z_{1/2}(E,\rho(z))(\ln 2)^{-1/m} \tag{6}$$

$$z_{1/2} = \frac{28.1}{\rho(z)} E^{1.71} \tag{7}$$

$P(z,E)$ is the positron implantation depth distribution as a function of the implantation energy E and the implantation depth z. Equations 4 and 5 are the Makhovian equation for $P(z,E)$, where z_0 is the mean implantation depth, which is dependent on the density and the width of the density gradient.[37]

The problem of fitting a density gradient $\rho(z)$ to the experimental beam data can be divided into two parts: (i) calculation of $P(z,E)$ as adjusted for the density gradient, i.e., eq 4, and (ii) calculation of the relationship between mass density and τ_3 by use of eq 3. Equation 2 can then be used to fit a density gradient to the experimental beam data.

(i) Adjusted Implantation Depth Distribution *P(z,E).* The presence of a density gradient alters the shape of $P(z,E)$, particularly if the mean implantation depth approaches the thickness of the density gradient. Figure 4 displays this effect in the case of a 2 nm density gradient and a 3 nm median implantation depth (e.g., 0.3 keV in PMMA).

Since the implantation depth is reciprocally dependent on the density, a decrease in density at the near-surface region leads to the implantation depths being greater. In the example shown in Figure 4, the median implantation depth at 0.3 keV increases by about 50% in the presence of the 2 nm wide density gradient. A

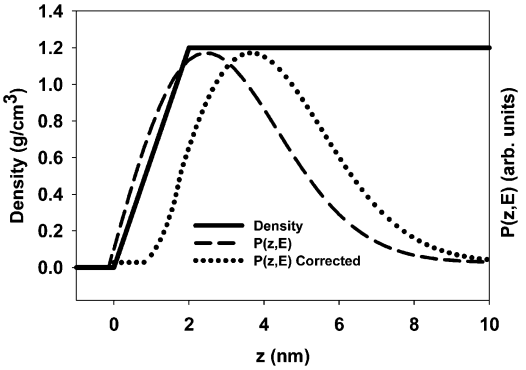

Figure 4. Makhovian implantation profile for positrons implanted at 0.3 keV in PMMA with a density gradient width of 2 nm. The broken line represents the uncorrected shape of the implantation depth distribution, and the dotted line represents the implantation depth distribution which has been corrected for the presence of the density gradient. In this example, the impact of the density gradient of 2 nm is an increase in the median implantation depth by ca. 50% (from 3 to 4.5 nm).

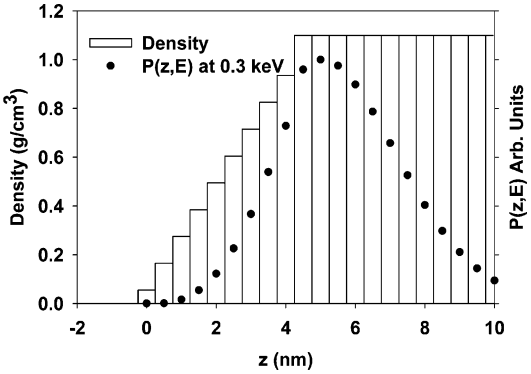

Figure 5. Linear density gradient is represented by a step function (vertical bars), together with the relative fraction of positrons stopped in each layer (●), as estimated by the density-gradient-adjusted Makhovian implantation depth distribution for positrons implanted at 0.3 keV.

density-adjusted $P(z,E)$ may be estimated using a previously derived concept employed in calculating the fraction of positrons thermalized in layers of differing density in multilayered samples.[60] Estimation of the fraction of positrons stopped within a depth range of constant density ρ_i involved use of

$$P(z,E) = -\frac{\mathrm{d}}{\mathrm{d}z}\left\{\exp\left[-\left(\frac{z-\delta_i}{z_{0i}}\right)^m\right]\right\} \tag{8}$$

in which δ_i is determined by the condition that the positron transmission T must be continuous at all z (eq 9).

$$T(z) = 1 - \int_0^z P(z,E)\, \mathrm{d}z \tag{9}$$

By approximating a density gradient $\rho(z)$ within the density gradient width z' by use of a step function of 10 steps, the fraction of positrons stopped in each layer could be calculated by use of eqs 8 and 9. This allowed a density gradient-adjusted $P(z,E)$ to be estimated. Figure 5 shows the step function representing the density gradient together with the positron implantation profile, adjusted for the same density gradient.

The τ_3 evaluated from such an implantation probe represents the average of the τ_3 obtained for each of the

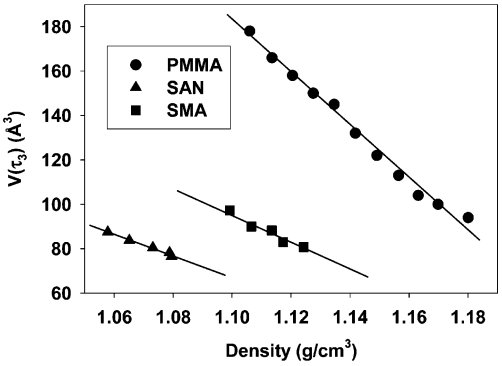

Figure 6. Free volume cavity size $V(\tau_3)$ as a function of density of PMMA, SAN, and SMA. $V(\tau_3)$ was obtained from conventional bulk PALS and eq 1, and the density was changed by varying the temperature (PMMA)[51,52] and by pressure densification (SAN, SMA).[61]

segments together with the relative fraction of positrons stopped each.

We assumed in the present study that the implantation characteristics in the low-energy range (0.3−3 keV) are constant, just as is found in the 3−18 keV range,[37] and used a value of $m = 2$ for the Makhovian implantation profile (eq 4). The most important inelastic event for the stopping of positrons in polymers is the ionization of the polymer segments in the energy range 10−20 eV, i.e., more than 1 order of magnitude smaller than the lowest implantation energy of 300 eV. It is reasonable to assume then that the cross section of the inelastic events is relatively energy independent within the implantation energy range used in the study.

The diffusion of positrons may have an effect on the lifetime spectra at energies for which the median implantation depth approaches the positron diffusion length. The typical large effects on the intensities in the low-energy range as displayed in Figure 2 have been attributed to the outward diffusion of positrons from the sample. The positron diffusion lengths have been quantified from I_3 in relation to the implantation energy data, resulting in estimates of the positron diffusion length in the nanometer range.[38,44,45]

The effects of positron and positronium diffusion on the average positron lifetime in the low-energy region have been little investigated. Since the o-Ps is generally thought to have a considerably shorter diffusion length than positrons, it can be assumed to be annihilated very close to where it is formed. The effect of positron diffusion on the o-Ps lifetime thus becomes closely linked to the hitherto unresolved question of when and where the o-Ps is formed in relation to the thermalization and diffusion of the positron. From Figure 2a,b it can be clearly seen that positrons implanted at 0.4 keV, corresponding to an implantation depth of 6 nm, form o-Ps and are annihilated at the normal bulk lifetime of approximately 2.0 ns. At that implantation energy, there is a clear reduction in I_3 in comparison to the bulk value. This can be interpreted as o-Ps being formed close to where the positron is thermalized and of its having a diffusion length which is much less than the median implantation depth of approximately 6 nm at 0.4 keV.

(ii) Relationship between Mass Density and τ_3. Data on the mass density and the o-Ps lifetime of all three polymers, obtained from previous work on identical materials,[51,52,61] are plotted in Figure 6.

A linear relationship was found between the mass density and the free volume cavity size as calculated

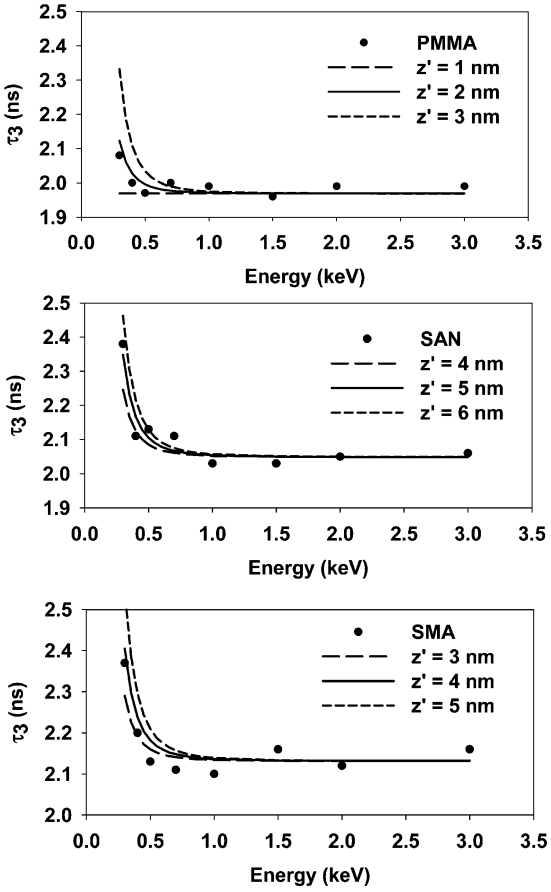

Figure 7. Values of τ_3 (●) for PMMA, SAN, and SMA (experimentally obtained from positron beam measurements), together with τ_3 predicted from the linear density gradient model as a function of the width of the density gradient z' (lines in graph).

Table 1. Linear Relationships between Mass Density and Free Volume Cavity Size Obtained from the o-Ps Annihilation Lifetime According to $V(\tau_3) = A\rho + b$

material	A [Å^3/(g/cm^3)]	b (Å^3)	R^2
PMMA	−1182	1483	0.9895
SAN	−471	586	0.9849
SMA	−652	813	0.9539

by eq 1, the parameters being listed in Table 1. The relationship between τ_3 and the free volume cavity size has been investigated for several materials. The equations and the values of the parameters as given in eq 1 can be used for o-Ps lifetimes of up to at least 10 ns, which covers most of the range of lifetimes used in the fitting of linear density gradient (>1000 Å^3).[62]

Fitting of Density Gradient Thickness to Experimental Data. Assuming a linearly increasing density gradient $\rho(z)$ with a width of z' (Figure 3), the free parameter z' was fitted to the experimental results shown in Figure 2. In Figure 7, τ_3, as shown as a function of the implantation energy for a particular width of the density gradient, is plotted together with the experimental data on τ_3. The results of the fitting are presented in Table 2.

The density gradient estimates shown in Table 2 can be conveniently compared to certain data of the density fluctuations of polymer surfaces from the literature. Although of great importance in understanding the nature of polymer surfaces, experimental data on the density gradients of polymer surfaces are scarce in the literature. However, results from two previous studies

Table 2. Density Gradient Widths of Amorphous Polymer Obtained by Use of a Low-Energy Positron Lifetime Beam, As Obtained from the Fitting of z' to the Experimental Beam Data in Figure 7

material	z' (nm)
PMMA	2 ± 0.5
SAN	5 ± 1
SMA	4 ± 1

can be compared with the present data. Neutron reflectivity has been used to measure density gradients in spin-cast PMMA obtained from an *o*-xylene solution.[63] Prior to proper annealing, a density gradient width of about 4.5 nm was obtained, whereas after annealing at a level above the T_g the width of the density gradient was reduced to a "sharp free polymer surface". Although quantitative data on the width of the density gradient after annealing had been performed were not provided, sensitivity of the density gradient to the annealing process was clearly demonstrated. X-ray reflectivity measurements have been used earlier for characterizing a thin film of spin-casted polystyrene. An "interface roughness" has been found at a with of only 0.32 nm.[64] This width is roughly the length of one monomer and must be considered as the lower limit of any density gradient for a polymer surface.

In this context, it is interesting to consider the dimensions of interfacial widths between immiscible pairs of polymers. The system of a vacuum−polymer interface would have some similarities to a polymer−polymer interface, in which case the two polymers are unable to interact and are completely incompatible. Generally, the interfacial width decreases with a decrease in miscibility,[65] and indeed the experimental data on the interfacial widths of polymer pairs appear to reach a minimum value of about 3 nm, e.g., for the interfacial width between PMMA and PS in the high molecular mass range.[66] This is in surprisingly close agreement with our estimate of a density gradient of about 2 nm for PMMA at a vacuum surface.

Density gradients of polymer surfaces have also been studied by use of Monte Carlo simulation, yielding sharp density gradients which can be conveniently compared with the values shown in Table 2. The width of the density gradients of glassy polymers has been calculated to be in the range 0.75−1 nm,[67,68] roughly corresponding to the length of three mers. Polymer melts have also been simulated in the same way using density gradient widths calculated to 2−3 times the segment diameter[69] or 1.5−4 nm.[70] Most of the results of these simulations thus suggest narrower density gradients than our estimates indicate, although they are still in reasonable agreement with the positron lifetime data of PMMA, the agreement being less in the case of SAN and SMA.

Predictions of Density Gradients from PVT Data. Density gradients for PMMA, SAN, and SMA were calculated from previously determined PVT data,[51,61] using the lattice fluid theory[54] in conjunction with the Cahn−Hilliard theory of inhomogeneous systems.[53] The Cahn−Hilliard theory has been developed for molecular interphases. It assumes that the interfacial free energy per molecule in the surface region depends on the sum of two components: (i) the local concentration, i.e., the free energy that the molecule would have in a homogeneous medium at that concentration, and (ii) the surrounding concentration, i.e., the derivative of the concentration gradient at that position in the gradient. The surface tension is the integral then over the sum of the two components, according to eq 10

$$\sigma = N_v \int_{-\infty}^{\infty} \left[\Delta a + \kappa \left(\frac{\mathrm{d}\rho}{\mathrm{d}x} \right)^2 \right] \mathrm{d}x \tag{10}$$

in which Δa is the free energy per molecule in a mixture of the two bulk phases, $\kappa(\mathrm{d}\rho/\mathrm{d}x)^2$ is the contribution per molecule of the concentration gradient, and x is the distance perpendicular to a flat interface. A large interphase width would result in a smaller gradient and reduce the free energy contribution of $\kappa(\mathrm{d}\rho/\mathrm{d}x)^2$, although the total number of molecules in the interphase contributing to the surface energy would increase. There is thus a particular shape and size of the gradient that yield a minimum of total surface energy σ. It can be shown that the surface energy σ is minimized by the condition

$$\Delta a = \kappa \left(\frac{\mathrm{d}\rho}{\mathrm{d}x} \right)^2 \tag{11}$$

Integration of eq 11 can be written in reduced (dimensionless) variables, yielding an expression which relates a given concentration to a distance from an arbitrarily chosen origin (eq 12):

$$\tilde{x} - \tilde{x}_0 = \int_{\tilde{\rho}_0}^{\tilde{\rho}} (\tilde{\kappa}/\Delta\tilde{a})^{1/2} \, \mathrm{d}\tilde{\rho} \tag{12}$$

In eq 12, $\tilde{x}_0$ is an arbitrarily chosen origin with a reduced density of $\tilde{\rho}_0$ ($\tilde{\rho}_g < \tilde{\rho}_0 < \tilde{\rho}_l$) and $\tilde{x} \equiv x/v^{*1/3}$, where v^* is the close-packed mer volume. Equation 12 calculates a distance in relation to the origin where this density is found for a particular density difference (e.g., the bulk density vs half of the bulk density). The distance is expressed in units of a close-packed mer volume v^* to the power of $^1/_3$. A value of $\tilde{\kappa} = 0.55$, which has previously been fitted to experimental data on polymers, was employed.[55]

$\Delta\tilde{a}$ can be estimated as a function of density from the Sanchez−Lacombe lattice fluid theory according to eq 13

$$\Delta\tilde{a} = \tilde{P}_e - \tilde{\rho}^2 + \tilde{T}[(1 - \tilde{\rho}) \ln(1 - \tilde{\rho}) + (\tilde{\rho}/r) \ln \tilde{\rho}] - \tilde{\rho}\tilde{\mu}_e \tag{13}$$

in which r is the number of mers/molecule. For high-molecular-mass polymers, the equilibrium vapor pressure $\tilde{P}_e = 0$. $\tilde{\mu}$ is the reduced chemical potential given by

$$\tilde{\mu} \equiv -\tilde{\rho} + \tilde{P}\tilde{v} + \tilde{T}\left[(\tilde{v} - 1) \ln(1 - \tilde{\rho}) + \frac{1}{r} \ln \tilde{\rho} \right] \tag{14}$$

The following equation of state defines the equilibrium which minimizes the chemical potential so that $\tilde{\mu} = \tilde{\mu}_e$:

$$\tilde{\rho}^2 + \tilde{P} + \tilde{T}[\ln(1 - \tilde{\rho}) + (1 - 1/r)\tilde{\rho}] = 0 \tag{15}$$

The definitions of v^*, $\tilde{P}$, $\tilde{v}$, $\tilde{T}$, P^*, and $T^*$are as follows:

$$\tilde{T} \equiv T/T^*, \quad T^* \equiv \epsilon^*/k \tag{16a, 16b}$$

$$\tilde{P} \equiv P/P^*, \quad P^* \equiv \epsilon^*/v^* \tag{17a, 17b}$$

$$\tilde{v} \equiv 1/\tilde{\rho} \equiv V/V^* \tag{18a, 18b}$$

P^*, V^*, and T^* are the experimentally determined Sanchez−Lacombe PVT scaling parameters as listed in

Table 3. Parameters of the Sanchez−Lacomb Equation of State Fitted to the PVT Data of Amorphous Polymers

material	P^* (MPa)	V^* (cm^3/g)	T^* (K)	T_g[a] (°C)	temp range used (°C)
PMMA	534.3	0.8018	702.8	105	110−190
SAN	440.3	0.8935	732.8	106	120−180
SMA	392.4	0.8631	760.3	126	130−180

[a] T_g by DMA (dynamical mechanical analysis) using a maximum of G''.

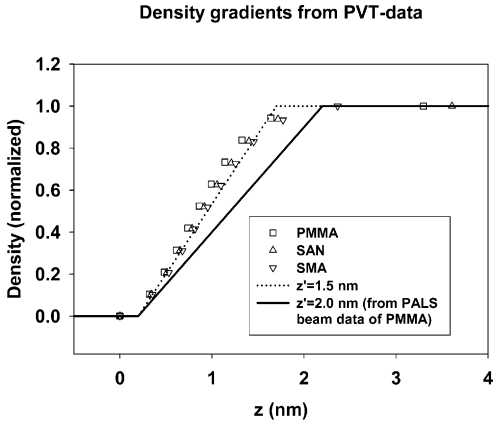

Figure 8. Density gradients calculated from PVT data of amorphous polymers using the Cahn−Hilliard theory of inhomogeneous systems in conjunction with the Sanchez−Lacombe lattice fluid theory. Linear density gradient widths of $z' = 1.5$ and 2 nm are also displayed (broken and solid line, respectively).

Table 2, and ϵ^* is the total interaction energy per mer. A more comprehensive account of all the equations used can be found in the earlier work of Poser et al.[55]

The approach employed here has been used previously to predict density gradients and surface tensions from PVT scaling parameters and has been shown to accurately predict surface tensions for a range of liquids and polymer melts.[55,71,72] The PVT data used, obtained from previously published work,[51,61] was measured by use of a Bellows-type instrument (Gnomix Inc. PVT apparatus). The Sanchez−Lacombe PVT scaling parameters were determined from the experimental data, using the evaluation program PVTEVAL V6.04. Table 3 displays the results of the fitting, using pressures of 0−200 MPa.

Figure 8 displays the results for all three polymers at room temperature. There are clearly only very small differences between the three polymers, probably due to their similar bulk properties such as those of glass transitions, polarities, and large molecular mass.

The resulting density gradients are sigmoidal in shape, which can be approximated using a linear density gradient with a thickness of about 1.5 nm. This is in excellent agreement with the earlier measurements of Dee et al.[72] Clearly, the theoretical predictions are in close agreement with the fitted density gradient of PMMA (about 2 nm) and to a somewhat lesser extent too with SAN and SMA (5 and 4 nm, respectively).

Discussion

The main reason for assuming simple linear density gradients in the study was to avoid using more than one fitting parameter. Although the limited amount of experimental data available and the simulations of polymer surfaces used to guide us in this respect suggest the density gradient to be of sigmoidal shape of rather than linear, more than one fitting parameter would be required, and we consider ourselves unable, also in view of experimental error, to determine which shape gives the better fit. A tempting alternative to the simple linear density gradients is use of a sharp density gradient in combination with a near-surface region of decreased density. Such a model would be in better agreement with the widely accepted notion of a near-surface region of increased mobility, and it could provide values of the parameters agreeing closely with certain previous measurements. For instance, the relatively large widths of our fitted density gradients could easily be reduced by assuming instead a slightly reduced density in a near-surface layer. Inevitably, however, two highly interdependent fitting parameters would have been introduced by use of such a model, parameters that could only be fitted quite arbitrarily. The contribution which the reporting of values that such a model would have provided would be doubtful. Despite its roughness, we thus consider the linear density gradient to represent a suitable model for describing our data. The widths of the density gradients as given in Table 2 are at least an indication of the dimensions of the true density gradients of the measured polymers.

The difference in the density gradient widths between the three polymers raises questions whether and to what extent the dimensions of the density gradient can be expected to be dependent on material and molecular mass. The difference in polarity between the polymers cannot explain the difference, since this would favor even sharper gradients for the slightly more polar SAN and SMA. It should be noted that the Cahn−Hilliard theory may fail for copolymers if there is a concentration of specific mers at the surface.[71] Both copolymers consist of highly polar groups (25% acrylonitrile and 14% maleic anhydride, respectively) copolymerized with the moderately polar styrene. Since there is a difference in the polarity of the polymer constituents, there may be some degree of orientation or an excess of one of the groups at the vacuum surface. The behavior of copolymers at a free vacuum surface has been studied previously by Sauer et al.[71] They measured the surface tension of a diblock copolymer poly[dimethylsiloxane-*co*-poly(ethylene oxide)] PDMS(0.25)/PEO(0.75) and a partially flourinated alkane ($CF_3CF_2CF_2(CH_2)_8CH_3$). They found that the surface tension of each polymer was considerably lower than predicted from the bulk properties. This was attributed to the excess of the low-energy constituents at the vacuum surface. Such an orientation at the vacuum surface of SMA and SAN might significantly influence the density gradients as characterized in the present study.

An implicit assumption in the Cahn−Hilliard theory is that the composition gradient should be small in relation to the reciprocal of the intermolecular distance. The average composition gradient can be estimated to $1/1.5 = 0.67$ nm^{-1} (Figure 8). This is in fact smaller than the reciprocal of the intermolecular distance in PMMA, which can be estimated to 2 nm^{-1} by calculating a mer volume to 140 Å^3/mer from the bulk density of 1.19 g/cm^3 and a molar weight of each mer equal to 100 g/mol. From this simple observation, one can also conclude that a gradient width of 1.5 nm as obtained in this study (Figure 8) is the length of only three mers.

In this context, it is instructing to consider the Kuhn segment chain lengths for PMMA, i.e., the minimum numbers of mers that are needed to travel along a

polymer backbone so that the effects of the orientation of the first mer has vanished. For PMMA, the Kuhn segment chain length has been quantified to six mers,[73] corresponding to a full length of roughly 1.8 nm along the polymer backbone. This is actually in surprisingly good agreement with the estimated density gradient width of 2 nm from the positron beam results. Other quantitative estimates such as the persistence length, albeit for stereoregular PMMA, are in the range of a few nanometers,[74,75] also suggesting that the short-range order in PMMA is of the same length scale as the width of the density gradient. One could in this sense also picture the occurrence of density gradients arising from the limited ability of the polymer segments to form a flat interphase due to chain stiffness and steric hindrance.

It is of interest to compare the density gradient widths obtained in the present study with some of the numerous studies of surface-influenced glass transition temperatures of polymers as reviewed in the Introduction section. Perhaps the most important observation, most recently pointed out by Jones,[77] is the discrepancy between the length scale of the surface effects on density and glass transition, respectively, when moving from the surface into the bulk state of the polymer. As has been shown in the present study, the effects on density by the presence of the surface vanish at depths of only a few nanometers into the polymer (or at even at shorter distances from the surface according to the limited number of previous experimental studies[49,50,63,64]). This is in contrast to the surface effects on T_g, which is often found to be depressed in a layer of ca. 10 nm or more from the surface. Thus, the relation between density (or free volume) and T_g does not seem to be straightforward at polymer surfaces; i.e., $T_g(z)$ is not a unique function of $\rho(z)$.

One reason for the discrepancy between the length scale of the surface effects on the density and T_g could be that the local $T_g(z)$ is dependent not only on the local density $\rho(z)$ but also on the density of the surrounding. This is expected due to the fact that the α-relaxation processes responsible for the glass transition occur by the cooperative movement of several polymer segments, characterized by some length ξ. The size of such an element is in the range of a few nanometers, which puts an upper limit to how much T_g can change per distance unit at e.g. the vicinity of a surface. However, the effects on T_g are found up to several tens of nanometers below the free surface, implying that there exists some additional mechanism for the surface effects to propagate through the polymer. An important aspect of the dynamics of amorphous polymers has recently been emphasized by Ellison and Torkelson,[76] who stressed that regions of fast dynamics are unlikely to be close to regions of very slow dynamics, i.e., that a change in dynamics is unlikely to occur abruptly anywhere in the polymer, e.g., a free polymer surface. Such a strong coupling between the dynamics of adjoining polymer segments would thus put an even lower limit on how much T_g can change per distance unit. The T_g depression at polymer surfaces would in this case be dependent on the coupling between many adjoining polymer segments. One would thus expect an increasing reduction of T_g at constant film thickness as a function of chain stiffness (T_g) for a series of different polymers.

Conclusions

Positron lifetime spectra of PMMA, SAN, and SMA were recorded in the energy range 0.3−3.0 keV. A slight increase in τ_3 was observed in the low-energy range for each of them. Linear density gradients were fitted to the experimental beam data by the extrapolation of known implantation characteristics to the low-energy range and by assuming that positron and positronium diffusion did not influence τ_3. Density gradients with a width of 2, 5, and 4 nm were estimated for PMMA, SAN, and SMA, respectively. Excellent agreement was found between the estimated density gradient of PMMA and predictions based on PVT data as well as reasonable agreement with the Monte Carlo simulation of glassy surfaces. A wider density gradient was found for the copolymers. This may be an effect of surface orientation of the less polar groups, resulting in a decrease in surface tension and a broader interface region from the vacuum surface to the true bulk state.

The widths of the density gradients are smaller than the depth range of effects on T_g by the presence of the surface as reported in the literature. This discrepancy is believed to arise due to the fact that the local T_g is dependent not only on the local density but is also sensitive to the density of the surrounding as well as a strong coupling between the dynamics of adjoining polymer segments as recently suggested by Ellison and Torkelson.[76]

Acknowledgment. We thank the Scandinavia-Japan Sasakawa Foundation for their financial contribution and Swedish Research Council for funding this project.

References and Notes

(1) Orts, W. J.; van Zanten, J. H.; Wu, W. L.; Satija, S. K. *Phys. Rev. Lett.* **1993**, *71*, 867−870.
(2) Keddie, J. L.; Jones, R. A. L.; Cory, R. A. *Faraday Discuss.* **1994**, *98*, 219−230.
(3) Keddie, J. L.; Jones, R. A. L.; Cory, R. A. *Europhys. Lett.* **1994**, *27*, 59−64.
(4) Grohens, Y.; Brogly, M.; Labbe, C.; David, M. O.; Schultz, J. *Langmuir* **1998**, *14*, 2929−2932.
(5) Kim, J. H.; Jang, J.; Zin, W. C. *Langmuir* **2000**, *16*, 4064−4067.
(6) Fryer, D. S.; Peters, R. D.; Kim, E. J.; Tomaszewski, J. E.; de Pablo, J. J.; Nealey, P. F.; White, C. C.; Wu, W. L. *Macromolecules* **2001**, *34*, 5627−5634.
(7) Tsui, O. K. C.; Zhang, H. F. *Macromolecules* **2001**, *34*, 9139−9142.
(8) Kim, J. H.; Jang, J.; Zin, W. C. *Langmuir* **2001**, *17*, 2703−2710.
(9) Kawana, S.; Jones, R. A. L. *Phys. Rev. E* **2001**, *63*, 021501-1.
(10) Wallace, W. E.; Van Zanten, J. H.; Wu, W. L. *Phys. Rev. E* **1995**, *52*, R3329−R3332.
(11) van Zanten, J. H.; Wallace, W. E.; Wu, W. L. *Phys. Rev. E* **1996**, *53*, R2053−R2056.
(12) Forrest, J. A.; Dalnoki-Veress, K.; Stevens, J. R.; Dutcher, J. R. *Phys. Rev. Lett.* **1996**, *77*, 2002−2005.
(13) Forrest, J. A.; Dalnoki-Veress, K.; Dutcher, J. R. *Phys. Rev. E* **1997**, *56*, 5705−5716.
(14) Wu, W. L.; van Zanten, J. H.; Orts, W. J. *Macromolecules* **1995**, *28*, 771−774.
(15) Pochan, D. J.; Lin, E. K.; Satija, S. K.; Wu, W. L. *Macromolecules* **2001**, *34*, 3041−3045.
(16) Prucker, O.; Christian, S.; Bock, H.; Ruhe, J.; Frank, C. W.; Knoll, W. *Macromol. Chem. Phys.* **1998**, *199*, 1435−1444.
(17) Fukao, K.; Miyamoto, Y. *Europhys. Lett.* **1999**, *46*, 649−654.
(18) Fukao, K.; Miyamoto, Y. *Phys. Rev. E* **2000**, *61*, 1743−1754.
(19) Fukao, K.; Uno, S.; Miyamoto, Y.; Hoshino, A.; Miyaji, H. *J. Non-Cryst. Solids* **2002**, *307*, 517−523.
(20) Forrest, J. A.; Mattsson, J. *Phys. Rev. E* **2000**, *61*, R53−R56.

(21) DeMaggio, G. B.; Frieze, W. E.; Gidley, D. W.; Zhu, M.; Hristov, H. A.; Yee, A. F. *Phys. Rev. Lett.* **1997**, *78*, 1524−1527.
(22) Satomi, N.; Takahara, A.; Kajiyama, T. *Macromolecules* **1999**, *32*, 4474−4476.
(23) Hammerschmidt, J. A.; Gladfelter, W. L.; Haugstad, G. *Macromolecules* **1999**, *32*, 3360−3367.
(24) Ge, S.; Pu, Y.; Zhang, W.; Rafailovich, M.; Sokolov, J.; Buenviaje, C.; Buckmaster, R.; Overney, R. M. *Phys. Rev. Lett.* **2000**, *85*, 2340−2343.
(25) Wang, X. P.; Xiao, X.; Tsui, O. K. C. *Macromolecules* **2001**, *34*, 4180−4185.
(26) Bliznyuk, V. N.; Assender, H. E.; Briggs, G. A. D. *Macromolecules* **2002**, *35*, 6613−6622.
(27) Fischer, H. *Macromolecules* **2002**, *35*, 3592−3595.
(28) Kajiyama, T.; Tanaka, K.; Takahara, A. *Macromolecules* **1997**, *30*, 280−285.
(29) Tanaka, K.; Taura, A.; Ge, S.-R.; Takahara, A.; Kajiyama, T. *Macromolecules* **1996**, *29*, 3040−3042.
(30) Kajiyama, T.; Tanaka, K.; Takahara, A. *Polymer* **1998**, *39*, 4665−4673.
(31) Johannsmann, D. *Eur. Phys. J. E* **2002**, *8*, 257−259.
(32) Jones, R. A. L. *Curr. Opin. Colloid Interface Sci.* **1999**, *4*, 153−158.
(33) Forrest, J. A.; Dalnoki-Veress, K. *Adv. Colloid Interface Sci.* **2001**, *94*, 167−196.
(34) Forrest, J. A. *Eur. Phys. J. E* **2002**, *8*, 261−266.
(35) Bauer-Kugelmann, W.; Sperr, P.; Kogel, G.; Triftshauser, W. *Positron Annihilation* **2001**, *363-3*, 529−531.
(36) Suzuki, R.; Ohdaira, T.; Mikado, T. *Radiat. Phys. Chem.* **2000**, *58*, 603−606.
(37) Algers, J.; Sperr, P.; Egger, W.; Kogel, G.; Maurer, F. H. J. *Phys. Rev. B* **2003**, *67*, 125404.
(38) Xie, L.; DeMaggio, G. B.; Frieze, W. E.; DeVries, J.; Gidley, D. W.; Hristov, H. A.; Yee, A. F. *Phys. Rev. Lett.* **1995**, *74*, 4947−4950.
(39) Jean, Y. C.; Zhang, R.; Cao, H.; Yuan, J.-P.; Huang, C.-M.; Nielsen, B.; Asoka-Kumar, P. *Phys. Rev. B* **1997**, *56*, R8459−R8462.
(40) He, C.; Suzuki, T.; Hamada, E.; Kobayashi, H.; Kondo, K.; Shantarovich, V. P.; Ito, Y. *Mater. Res. Innov.* **2003**, *7*, 37−41.
(41) He, C.; Hamada, E.; Suzuki, T.; Kobayashi, H.; Kondo, K.; Shantarovich, V. P.; Ito, Y. *J. Radioanal. Nucl. Chem.* **2003**, *255*, 431−435.
(42) Miyamoto, K.; Terashima, Y.; Tashiro, M.; Honda, Y.; Tagawa, S. *J. Photopolym. Sci. Technol.* **2003**, *16*, 411−412.
(43) Jean, Y. C.; Cao, H.; Dai, G. H.; Suzuki, R.; Ohdaira, T.; Kobayashi, Y.; Hirata, K. *Appl. Surf. Sci.* **1997**, *116*, 251−255.
(44) Cao, H.; Zhang, R.; Yuan, J.-P.; Huang, C.-M.; Jean, Y. C.; Suzuki, R.; Ohdaira, T.; Nielsen, B. *J. Phys.: Condens. Matter* **1998**, *10*, 10429−10442.
(45) Cao, H.; Yuan, J.-P.; Zhang, R.; Sundar, C. S.; Jean, Y. C.; Suzuki, R.; Ohdaira, T.; Nielsen, B. *Appl. Surf. Sci.* **1999**, *149*, 116−124.
(46) Uedono, A.; Suzuki, R.; Ohdaira, T.; Mikado, T.; Tanigawa, S.; Ban, M.; Kyoto, M.; Uozumi, T. *J. Polym. Sci., Part B: Polym. Phys.* **2000**, *38*, 101−107.
(47) Hamada, E.; Oshima, N.; Katoh, K.; Suzuki, T.; Kobayashi, H.; Kondo, K.; Kanazawa, I.; Ito, Y. *Acta Phys. Pol., A* **2001**, *99*, 373−378.
(48) Uedono, A.; Suzuki, R.; Ohdaira, T.; Uozumi, T.; Ban, M.; Kyoto, M.; Tanigawa, S.; Mikado, T. *J. Polym. Sci., Part B: Polym. Phys.* **1998**, *36*, 2597−2605.
(49) Wallace, W. E.; Beck Tan, N. C.; Wu, W. L.; Satija, S. *J. Chem. Phys.* **1998**, *108*, 3798−3804.
(50) Forrest, J. A.; Dalnoki-Veress, K.; Dutcher, J. R. *Phys. Rev. E* **1998**, *58*, 6109−6114.
(51) Schmidt, M.; Olsson, M.; Maurer, F. H. J. *J. Chem. Phys.* **2000**, *112*, 11095−11106.
(52) Schmidt, M.; Maurer, F. H. *J. Polymer* **2000**, *41*, 8419−8424.
(53) Cahn, J. W.; Hilliard, J. E. *J. Chem. Phys.* **1958**, *28*, 258−267.
(54) Sanchez, I. C.; Lacombe, R. H. *J. Phys. Chem.* **1976**, *80*, 2352−2362.
(55) Poser, C. I.; Sanchez, I. C. *J. Colloid Interface Sci.* **1979**, *69*, 539−548.
(56) Extrand, C. W. *Polym. Eng. Sci.* **1994**, *34*, 390−394.
(57) PATFIT-1998 Computer program, RISOE National laboratory, Denmark.
(58) Tao, S. *J. Chem. Phys.* **1972**, *56*, 5499−5510.
(59) Eldrup, M.; Lightbody, D.; Sherwood, J. N. *Chem. Phys.* **1981**, *63*, 51−58.
(60) Vehanen, A.; Saarinen, K.; Hautojärvi, P.; Huomo, H. *Phys. Rev. B* **1987**, *35*, 4606−4610.
(61) Schmidt, M.; Maurer, F. H. J. *Macromolecules* **2000**, *33*, 3879−3891.
(62) Ito, K.; Nakanishi, H.; Ujihira, Y. *J. Phys. Chem. B* **1999**, *103*, 4555−4558.
(63) Wu, W. L.; Orts, W. J.; van Zanten, J. H.; Fanconi, B. M. *J. Polym. Sci., Part B: Polym. Phys.* **1994**, *32*, 2475−2480.
(64) Sanyal, M. K.; Basu, J. K.; Datta, A.; Banerjee, S. *Europhys. Lett.* **1996**, *36*, 265−270.
(65) Stamm, M.; Schubert, D. W. *Annu. Rev. Mater. Sci.* **1995**, *25*, 325−356.
(66) Schubert, D. W.; Stamm, M. *Europhys. Lett.* **1996**, *35*, 419−424.
(67) Mansfield, K. F.; Theodorou, D. N. *Macromolecules* **1990**, *23*, 4430−4445.
(68) Mansfield, K. F.; Theodorou, D. N. *Macromolecules* **1991**, *24*, 6283−6294.
(69) Kumar, S. K.; Russell, T. P.; Hariharan, A. *Chem. Eng. Sci.* **1994**, *49*, 2899−2906.
(70) Cifra, P.; Nies, E.; Karasz, F. E. *Macromolecules* **1994**, *27*, 1166−1171.
(71) Sauer, B. B.; Dee, G. T. *J. Colloid Interface Sci.* **1994**, *162*, 25−35.
(72) Dee, G. T.; Sauer, B. B. *J. Colloid Interface Sci.* **1992**, *152*, 85−103.
(73) Bershtein, V. A.; Egorov, V. M.; Egorova, L. M.; Ryzhov, V. A. *Thermochim. Acta* **1994**, *238*, 41−73.
(74) Yamakawa, H. *Annu. Rev. Phys. Chem.* **1984**, *35*, 23−47.
(75) Grohens, Y.; Hamon, L.; Spevacek, J.; Holl, Y. *Macromol. Symp.* **2003**, *203*, 155−164.
(76) Ellison, C. J.; Torkelson, J. M. *Nature Mater.* **2003**, *2*, 695−700.
(77) Jones, R. A. L. *Nature Mater.* **2003**, *2*, 645−646.

MA0359335